Inorganic Chemistry

pubs.acs.org/IC

Article

The Covalent Au^I–Au^I Bond in $(AuF)_n$ (n = 2∼4): A Perspective to Understand the Closed-Shell Au^I···Au^I Interaction

Xinlei Yu, Dan Li, Kun Wang,* Tao Xia, Chang Xu, Zhenyu Wu, and Longjiu Cheng*

Cite This: *Inorg. Chem.* 2022, 61, 1051−1058

Read Online

ACCESS | Metrics & More | Article Recommendations | Supporting Information

ABSTRACT: The nature of closed-shell Au^I···Au^I attraction is still a conundrum in theoretical chemistry. However, for Au_2F_2 with a zigzag conformation, the d^{10}–d^{10} closed-shell interaction between the AuF monomers is demonstrated as a coordinate covalent bond. Chemical bonding analysis reveals that the strong Au^I···Au^I attraction is caused by the participation of the extraordinary active 5d orbital of Au. Based on our study, one of the 5d orbitals of the Au atom is activated to hybridize with its 6s and 6p orbitals to form hybridized dsp^2 orbitals, where each Au atom is both an electron donor (Lewis base) and acceptor (Lewis Acid) in dimerization. Actually, the closed-shell Au^I···Au^I interaction in the zigzag conformation of Au_2X_2 (X = F, Cl, Br, I, or NH_2) is covalent. Our results provide a rather simple but clear-cut example, where mysterious Au^I···Au^I attractions can be possibly explained by the covalent bond theory.

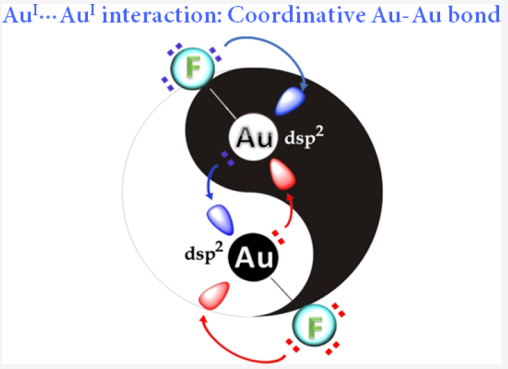

INTRODUCTION

Gold halides always display special chemical properties compared with other lighter coinage metal halides,[1−6] where the strong relativistic effects of an Au atom expand the inner 5d orbital and decrease the size of the 6s orbital. Many previous studies demonstrate that the bonding characters of Au−X bonds (X = F∼I) are both ionic and covalent, in which the covalent contribution is increased for Au−X interactions down the periodic table for halogens.[7−12] However, the polymers of coinage metal halides attract many investigations because of their diverse polymerization patterns, such as the D_{2h} symmetric Au_2F_2 (**1r**) formed by four equally covalent Au−F bonds[13] (Figure 1a). Different from **1r**, the C_{2v} symmetric Au_2F_2 (**1t**) is stabilized by the attraction between two closed-shell Au^I species (Figure 1b), where the Au−Au bond length is 2.56 Å under the theoretical level of B97D/QZVP.[14] In Figure 1, we have optimized **1r** and **1t** under the level of zero-order-regular approximation (ZORA)-TPSS-D3/dhf-QZVPP-2c based on previous studies.

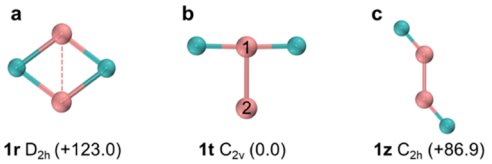

Figure 1. Three optimized isomers of Au_2F_2 under the level of ZORA-TPSS-D3/dhf-QZVPP-2c. (a) Rhombic (**1r**), (b) T-shaped (**1t**), and (c) zigzag (**1z**) Au_2F_2 structures Pink: Au; Green: F. Symmetry has been labeled for each structure. Enclosed is the single-point energy (in kJ/mol) under the level of DKH2-CCSD(T)/cc-pVTZ-DK/SO based on each optimized geometry.

Moreover, there are mysterious but widespread closed-shell metal−metal (M−M) interactions, such as the strong attractions between linearly two-coordinate gold atoms in the +1 oxidation state (Au^I) in molecular gold compounds.[15,16] Au^I is a closed-shell species with a $5d^{10}$ electronic configuration, with no space for the formation of the covalent Au^I···Au^I bond. These unusual Au^I···Au^I strong closed-shell interactions attract significant attention in gold chemistry.[17−28] In such systems, the observed Au^I···Au^I equilibrium distances (R) are in the range ca. 2.50−3.50 Å, well below the van der Waals distance (3.80 Å), and often below the nearest-neighbored distance in cubic close-packed gold metal (2.89 Å). The interaction energy of the Au^I···Au^I interaction is even up to 12 kcal/mol,[15] which is much stronger than van der Waals interactions and comparable with strong hydrogen bonds. Similar strong closed-shell interactions are also found in some other transition metals such as Cu^I, Ag^I, Hg^{II}, and Au^{III}, which is a phenomenon known as metallophilicity.[29−36]

The nature of closed-shell Au^I···Au^I attraction has been strongly debated ever since the pioneering theoretical study by the Hoffmann's group on Au^I···Au^I complexes.[37] Based on extended Hückel calculations, Hoffmann et al.[38] thought that

Received: October 11, 2021
Published: December 29, 2021

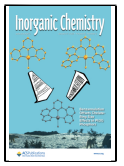

https://doi.org/10.1021/acs.inorgchem.1c03151
Inorg. Chem. 2022, 61, 1051−1058

the unusual interaction was due to the hybridization between 5d and 6s6p orbitals of gold. However, Pyykkö and Zhao[39] found that there is no closed-shell attraction in perpendicular $(ClAuPH_3)_2$ using the Hartree−Fork (HF) level. However, the attraction is observed with the second-order Møller-Plesset (MP2) method, suggesting that the $Au^I\cdots Au^I$ aurophilic interactions should be originated from electron correlation effects. Later studies revealed an R^{-6} behavior at large R in the equation for describing van der Waals interactions, directly suggesting that this interaction was a dispersion interaction. The coupled cluster singles and doubles with perturbative triples [CCSD(T)] calculations demonstrated that MP2 tends to overestimate the interaction.[25] From the analysis of local MP2 excitations for the perpendicular $(ClAuPH_3)_2$, Magnko et al.[40] found that about one-half of the post-HF attractions are originated from dispersion-type excitations, while the rest came from ionic contributions. However, many results from the density functional theory (DFT) methods with dispersion correction give contrast conclusions that dispersion is not the determining factor in aurophilicity.[41] Moreover, the prevalence $Au^I\cdots Au^I$ interactions are attributed to the relativistic enhancement of the strong electron affinity of Au.[42,43] On the basis of Che's results, the repulsion between two metal atoms/ions is balanced by the dispersion and electrostatic interaction of ligands.[44]

Here, we compare three isomerized dimers of AuF (Figure 1) to understand the relationship between two closed-shell Au^I species. Especially for zigzag Au_2F_2 (Figure 1c), we demonstrate that the nature of closed-shell $Au^I\cdots Au^I$ attraction is covalent. Then, we apply the viewpoint to explain the nature of $Au^I\cdots Au^I$ attraction in a series of clusters of $(AuX)_n$ (n = 2∼4) and M^I-M^I closed-shell attractions in $(MX)_2$, where M = Ag, Cu and X = F, Cl, Br, I, or NH_2.

COMPUTATIONAL METHODS

On the basis of benchmark calculations (Section 2 in the Supporting Information) in the NWChem 7.0.1 package,[45] all the geometric structures are optimized using TPSS exchange-correlation functional[46] with dispersion correction (D3) and dhf-QZVPP-2c[47,48] basis sets with the correction of spin-orbit (SO) coupling effects.[49] ZORA[50] is taken into consideration for the relativistic effects of coinage metals in optimization. Based on the optimized structures, the single-point energy and bonding energy (E_b) of Au_nX_n (X = F, Cl, Br, I, and NH_2, n = 2∼4) from the respective monomers are calculated under the DKH2-CCSD(T)/cc-pVTZ-DK/SO level with the basis set superposition error (BSSE) correction in Molpro 2020.1.[51,52]

In order to understand the electronic configurations, the analyses including electron localization function (ELF),[53] reduced density gradient (RDG) analysis,[54] Mayer bond order (MBO),[55,56] and Wiberg bond index (WBI) analysis[57] based on the optimized structures are completed by TPSS-D3(BJ)/dhf-QZVPP in the Gaussian 16 package[58] and Multiwfn tools (Version 3.7).[59] Visualization is performed using VMD 193 software.[60] As for the bonding analysis, each orbital has been confirmed by the natural bonding orbital (NBO) analysis using the adaptive natural density partitioning (AdNDP)[61] method under the level of TPSS-D3(BJ)/dhf-QZVPP.

In order to confirm the covalent nature of the closed-shell $Au^I\cdots Au^I$ attraction, the energy decomposition analysis (EDA) is carried out under the ZORA-TPSS-D3(BJ)/TZ2P (none frozen-core) level in ADF 2014.01.[62] The details of the methods and benchmark calculations have been summarized in Sections 1 and 2 of the Supporting Information.

RESULTS AND DISCUSSION

Three Isomers of Au_2F_2. We have confirmed the structures of Au_2F_2 based on the unbiased global search with the combination of the genetic algorithm (GA) and DFT. The details of the searching structures of Au_2F_2 have been summarized in Supporting Information Section 3.1. Three optimized structures of Au_2F_2 are shown in Figure 1.

1r is stabilized by four Au−F covalent bonds, but with an imaginary frequency of −162.2 cm^{-1} in our calculation. However, both **1t** and **1z** structures stabilized by closed-shell $Au^I\cdots Au^I$ attraction are the local minima on the energy surfaces, showing lower potential energy compared with the covalent-favored **1r** structure. The typical parameters of the three isomers are listed in Table 1.

Table 1. Bond Distance [R (Å)] of Au−Au and Au−F Bonds, Bond Angle [A (°)] of F−Au−Au for 1t and 1z or F−Au−F for 1r, NPA Charge [q_{Au} (e)] of Au, HOMO−LUMO Gaps of Different Isomers [E_{HL} (eV)], MBO, and WBI of Au−Au and Au−F Bonds under the Level of ZORA-TPSS-D3/dhf-QZVPP-2c

dimer	r (Å)	A (°)	q_{Au} (e)	E_{HL} (eV)	MBO	WBI
	Au−Au/Au−F				Au−Au/Au−F	Au−Au/Au−F
1r	2.62/2.25	109.1	+0.68	1.31	0.25/0.41	0.86/0.87
1t	2.52/1.93	91.2	+0.73(Au1)	1.24	0.90/0.70	1.49/1.50
			+0.43(Au2)			
1z	2.46/1.91	140.9	+0.52	1.36	1.03/0.85	1.77/1.58

In **1t** and **1z** structures, both the Au elements are in the +1 oxidation states but appear to have an unusual strong attraction to the other Au^I species, although Au_2F_2 (**1t**/**1z**) is different from the traditional aurophilic-determining structures of $(L-Au-X)_2$ (L = ligand).[16,38,63] However, similar to the competition between Au−I covalent bonding and Au−Au aurophilic interaction in the bond-bending isomerism of $Au_2I_3^-$,[64] the competition and isomerization between **1r** stabilized by covalent bonds and **1t**/**1z** stabilized by closed-shell attractions are studied based on the relaxed potential energy scan among **1r**, **1c**, and **1t** (Supporting Information Section 3.4). The detailed bonding analyses for **1r** and **1t** have been listed in Supporting Information section 4.

The Au−Au bond length is decreased from **1r** → **1t** → **1z**, but with increased covalent components reflected by the MBO and the WBI.

As for **1t** with the lowest potential energy of the three, both Au atoms are in the +1 oxidation states. [F−Au1−F] is an electronegative fragment, where the negative charge is from Au2 species and divided equally by two F atoms. Then, the whole molecule can be represented as $[F^{\delta-}-Au1^{\delta+}-F^{\delta-}]^{\delta-}Au2^{\delta+}$. Au1 adopts inequivalent dsp hybridization in forming one Au−Au σ bond and two Au−F σ bonds, which is consistent with the analysis of NPA charges shown in Table 1. The nature of closed-shell $Au^I\cdots Au^I$ attraction is a covalent coordinate bond of Au1(dsp) → Au2(6 s), which is confirmed by AdNDP analysis and ELF in Supporting Information Figure S5. In RDG analysis (Supporting Information Figure S5h), the value of the spike at −0.082 indicates the strong interaction between two Au^I species. Additionally, we do not find stable

https://doi.org/10.1021/acs.inorgchem.1c03151
Inorg. Chem. 2022, 61, 1051−1058

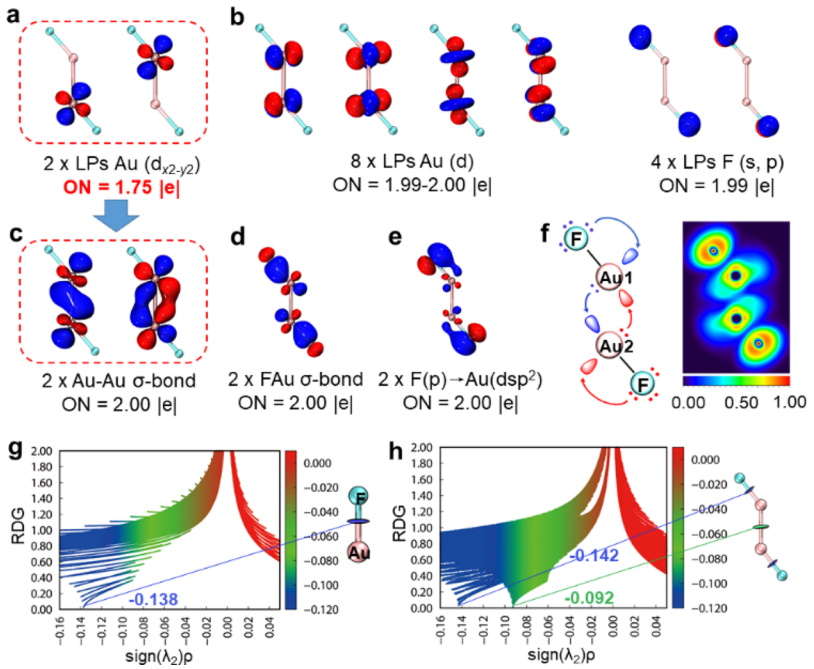

Figure 2. Bonding analysis of Au_2F_2 (**1z**). (a) Proposed localized $5d_{x2-y2}$ orbitals of Au. (b) Eight localized 5d orbitals of Au and four localized 2s/2p orbitals of F. (c) Two 2c−2e Au−Au coordinate covalent bonds formed by two dsp^2 orbitals of Au. (d) Two σ-type Au−F bonds. (e) Two coordinate F−Au bonds. (f) Lewis structure and ELF map of **1z**. (g,h) RDG plots for AuF and **1z** with the values of the spikes.

structures for other T-shaped Au_2X_2 (X = Cl, Br, and I) or M_2X_2 (M = Ag, Cu and X = F, Cl).

Coordinate Au^I−Au^I Bond of 1z. In the optimized zigzag Au_2F_2 (**1z**) shown in Figure 1c, the distance between two Au^I species is 2.46 Å, which is closer than that of **1t** (2.52 Å). The $Au^I\cdots Au^I$ attraction is 85.9 kJ/mol with BSSE correction under the level of DKH2-CCSD(T)/cc-pVTZ-DK/SO, based on the definition of the dissociation of Au_2F_2 (**1z**) → 2 AuF. Different from **1t**, 5d orbitals of both two Au species in Au_2F_2 (**1z**) are activated to participate in the hybridization with 6s and 6p orbitals based on the AdNDP results (Figure 2a∼e). For both the Au atoms, we notice that the ON values of LPs localized on both the $5d_{x2-y2}$ orbitals are only 1.75 |e| (Figure 2a), rather than 2.00 |e| of other eight localized 5d orbitals of Au atoms (Figure 2b). However, the ON values increase to 2.00 |e| when treating the molecular orbital formed by a pair of $5d_{x2-y2}$ orbitals as a 2-centers-2-electron (2c−2e) bond (Figure 2c), indicating that both the $5d_{x2-y2}$ orbitals participate in the Au−Au bonding. The results (Figure 2c) suggest that the Au−Au interaction is obviously a covalent double bond, including σ-type and π-type bonds.

Hence, we conclude that each Au atom adopts inequivalent dsp^2 hybridization and obtain the Lewis structure of Au_2F_2 (**1z**), which is consistent with the result of the ELF analysis shown in Figure 2f. Therefore, each Au^I species is amphoteric in **1z**, acting as both Lewis base (LPs donor) and Lewis acid (LPs acceptor) at the meantime.

Also, in addition to the two traditional σ(F−Au) bonds shown in Figure 2d, there are extra coordinate covalent bonds between Au and neighbored F atoms caused by the symmetry matching of orbitals, where the LPs of the F atom are donated to the empty dsp^2 orbital of the Au atom shown in Figure 2e. The extra ligand−metal coordinate covalent bond is reflected in the RDG analysis shown in Figure 2g,h. The spike at −0.142 shown in Figure 2h indicates that the Au−F interaction in **1z** is stronger than that of monomer AuF (−0.138) shown in Figure 2g.

In summary, the four inequivalent dsp^2 orbitals of each Au^I species participate in forming one σ(F−Au) bond, one π(F → Au) coordinate bond, one Au1(donor)−Au2(acceptor) coordinate bond, and one Au1(acceptor)−Au2(donor) coordinate bond. Therefore, the nature of aurophilic interactions can be viewed as the dsp^2=dsp^2 coordinate covalent double bond between two cooperative Lewis acid−base pairs. Therefore, RDG analysis shown in Figure 2h indicates that the coordinate $Au^I\cdots Au^I$ interaction in **1z** (with the value of spike at −0.092) is stronger than the single coordinate $Au^I\cdots Au^I$ bond of the **1t** structure (spike at −0.082 in Supporting Information Figure S5h).

Hence, we believe that ligand−metal interaction consolidates the hybridization of (n−1)d, ns, and np orbitals, which further enhances the closed-shell interactions. First of all, the F atom in **1z** with the strongest electronegativity induces Au to generate a σ hole when forming the σ(F−Au) bond, where the valence electrons of the Au atom is easy to be activated for the hybridization caused by its strong relativistic effect. Second, the symmetry of one of the 2p orbitals of F matches the symmetry of one of the dsp^2 orbitals of Au, where the F atom is able to donate LPs to empty the hybridized orbital of Au to consolidate the dsp^2 hybridization and strengthen the Au−Au interaction.

To demonstrate the strengthened effect of ligands, we design three isomers of $Au_2(NH_2)_2$ (Figure 3a∼c) similar to the isomers of Au_2F_2, including $Au_2(NH_2)_2$ (**Nz1**) with axial N−H bonds (Figure 3a), $Au_2(NH_2)_2$ (**Nz2**) with equatorial N−H bonds (Figure 3b), and a rhombic isomer (Figure 3c), where **Nz1** is the most stable one in the three isomers.

The potential energy indicates that **Nz1**/**Nz2** stabilized by closed-shell $Au^I\cdots Au^I$ attraction is more stable than **Nr**, which is stabilized by Au−N covalent bonds. All the isomers of

https://doi.org/10.1021/acs.inorgchem.1c03151
Inorg. Chem. 2022, 61, 1051−1058

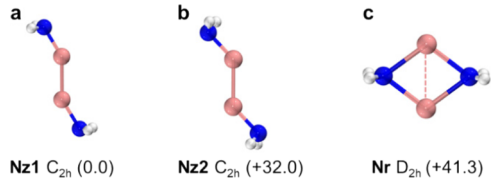

Figure 3. Three structures of $Au_2(NH_2)_2$ optimized under the ZORA-TPSS-D3/dhf-QZVPP-2c level. (a) C_{2h} symmetry zigzag $Au_2(NH_2)_2$ with axial N−H bonds (**Nz1**); (b) C_{2h} symmetry zigzag $Au_2(NH_2)_2$ with equatorial N−H bonds (**Nz2**) (c) D_{2h} symmetry rhombic $Au_2(NH_2)_2$ (**Nr**). Enclosed are the single point energies (kJ/mol) under the level of DKH2-CCSD(T)/cc-pVTZ-DK/SO based on the optimized geometries.

$Au_2(NH_2)_2$ are summarized in Supporting Information Figure S1.

The parameters of geometries and electronic configurations are summarized in Table 2. The Au−Au bond length of **Nz1** is shorter than that of **Nz2**. However, the larger WBI and MBO values of Au−Au bond in **Nz1** suggest its stronger covalent property compared with **Nz2**.

Table 2. Bond Distance [*R* (Å)] of Au−Au and Au−F Bonds, Bond Angle [*A* (°)] of N−Au−Au for Nz1 and Nz2 or N−Au−N for Nr, NPA Charge [q_{Au} (e)] of Au, HOMO−LUMO Gaps of Different Isomers [E_{HL} (eV)], MBO, and WBI of Au−Au and Au−N Bonds under the Level of ZORA-TPSS-D3/dhf-QZVPP-2c

structure	*r* (Å)	*A* (°)	q_{Au} (e)	E_{HL} (eV)	MBO	WBI
	Au−Au/Au−N				Au−Au/Au−N	Au−Au/Au−N
Nz1	2.49/1.97	149.4	0.28	1.64	0.82/0.90	1.64/1.41
Nz2	2.52/1.99	136.1	0.30	1.81	0.72/0.81	1.54/1.32
Nr	2.65/2.22	106.8	0.46	1.54	0.15/0.53	0.94/0.87

We analyze the bonding structures using AdNDP methods for **Nz1** and **Nz2** to understand the effect of ligands on structural stabilization, as shown in Figure 4. In addition to the similar coordinate nature of Au−Au interactions (boxed in Figure 4a,b), the difference between **Nz1** and **Nz2** is the relationship between ligands and the center metal. For $Au_2(NH_2)_2$ (**Nz1**) shown in Figure 4a, the amino with axial N−H bonds satisfies symmetry matching between the N 2p orbital and the Au dsp^2 orbital. Hence, the nature of the Au−N interaction contains the σ(N−Au) bond and the π-type coordinate bond. However, for $Au_2(NH_2)_2$ (**Nz2**) shown in Figure 4b, with equatorial N−H bonds, LPs of the N atom cannot be donated to the empty dsp^2 orbital of Au, leading to lower MBO/WBI results shown in Table 2. The electronic structures of **Nz1** and **Nz2** can be described as the Lewis structures, as shown in Figure 4c. Thus, the Au−Au bond distance of **Nz2** is elongated to 2.52 Å. The closed-shell interaction (defined as the dissociation of $Au_2(NH_2)_2$ (**1z**) → 2 $AuNH_2$ of **Nz1** is 32.0 kJ/mol lower than that of **Nz2**, consistent with the results of WBI.

On the basis of RDG analysis shown in Figure 4d,e, the value of the spike for the Au−N bond is −0.148 in the monomer $AuNH_2$, which is decreased to −0.157 in **Nz1** and −0.154 in **Nz2**, indicating that the Au−N interaction is enhanced in **Nz1** because of the additional π-type coordinate Au−N bond.

The value of the spike at −0.082 of **Nz1** is lower than −0.072 of **Nz2**, indicating the Au···Au interaction in **Nz1** is strengthened by the enhanced ligand−metal interactions. Therefore, **Nz1** with both σ- and π-type Au−N bonds appears to be shorter Au−Au distance and stronger closed-shell interaction, demonstrating that the stronger ligand−metal interactions consolidate the dsp^2 hybridization of Au^I species to strengthen the coordinate Au═Au bond.

In order to confirm the metallophilicity of different coinage metal halides with similar structures, we scan the potential energy for the transformation among the zigzag, T-shaped, and rhombic structure of Au_2Cl_2 and other M_2X_2 (M = Cu, Ag; X = F, Cl) in Supporting Information Sections 5 and 6. Similarly, the nature of the closed-shelled Au^I−Au^I interaction is the coordinate covalent bond in T-shaped Au_2Cl_2 and the coordinate covalent double bond in zigzag Au_2Cl_2. For the

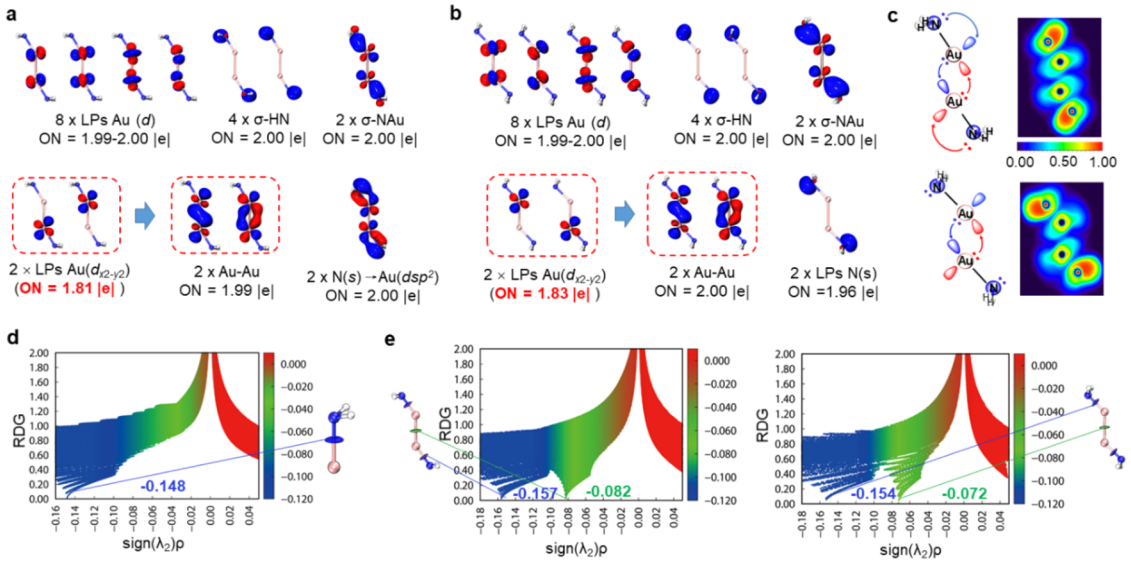

Figure 4. Bonding analysis of $Au_2(NH_2)_2$ (**Nz1** and **Nz2**) (a) AdNDP analysis for **Nz1**. (b) AdNDP analysis for **Nz2**. (c) Lewis structures and ELF maps of **Nz1** and **Nz2**. (d) RDG plots for monomer $AuNH_2$. (e) RDG plots for **Nz1** and **Nz2**.

https://doi.org/10.1021/acs.inorgchem.1c03151
Inorg. Chem. 2022, 61, 1051−1058

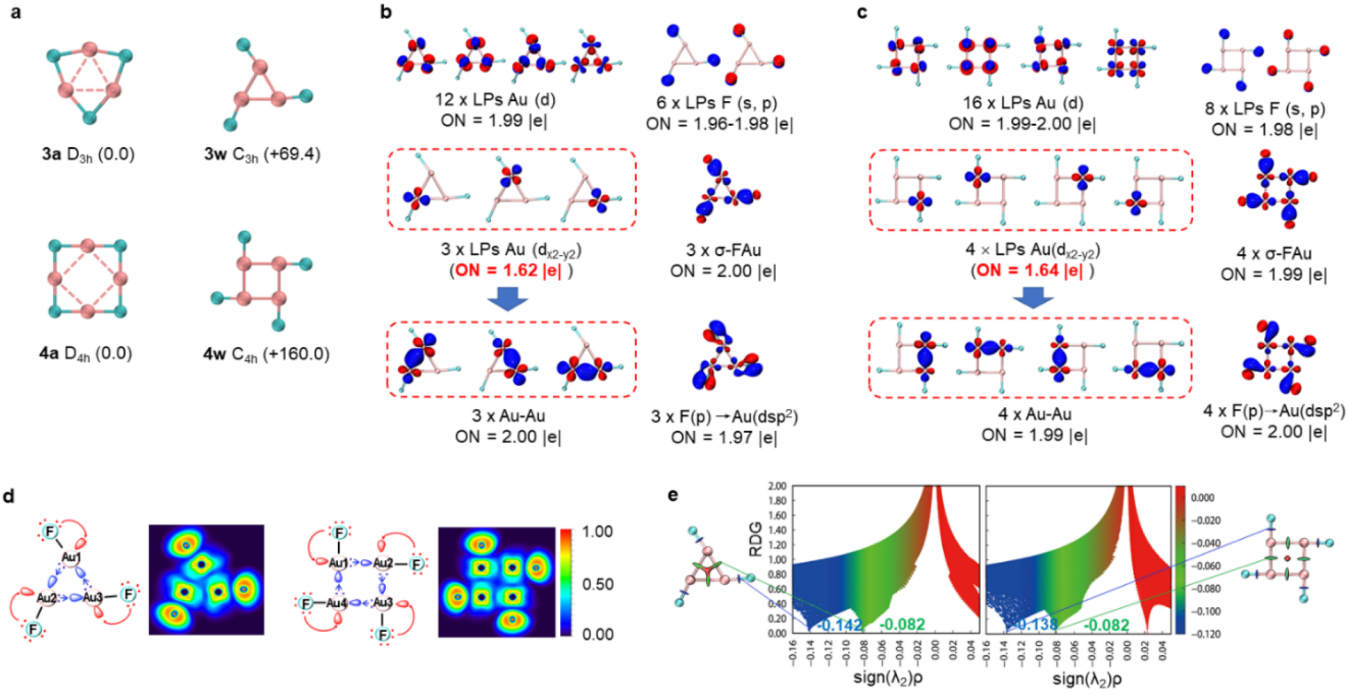

Figure 5. Electronic structures, AdNDP analysis, and RDG analysis for Au_3F_3 and Au_4F_4. (a) Optimized structures for annular isomers (**3a** and **4a**) and windmill-shaped isomers (**3w** and **4w**) with their geometric symmetries. Enclosed are the single point energies (kJ/mol) under the level of DKH2-CCSD(T)/cc-pVTZ-DK/SO. (b) AdNDP analysis for **3w**. (c) AdNDP analysis for **4w**. (d) Lewis structures and ELF Maps of **3w** and **4w**. (e) RDG plots for **3w** and **4w**.

dimers of coinage metal halides (M_2X_2, M = Cu, Ag; X = F, Cl), we do not find stable zigzag M_2X_2 (M = Cu, Ag; X = F, Cl), caused by the weak relativistic effect of Ag and Cu, where the inert d electrons are difficult to hybridize with valence s or p orbitals. Therefore, the zigzag structure can be only stabilized by the activated dsp^2 hybrid orbitals of the center metal, where dsp^2 hybridization in zigzag Au_2X_2 (X = F, Cl) can be consolidated with the enhanced participation of ligands.

We define the bonding energy (E_b) between two monomers in zigzag Au_2X_2 as the potential energy difference of $Au_2X_2 \rightarrow 2AuX$. In zigzag Au_2X_2 (X = F, Cl, Br, I), E_b of Au_2F_2 is 85.9 kJ/mol, which is larger than that of zigzag structures of Au_2Cl_2 (67.2 kJ/mol), Au_2Br_2 (66.5 kJ/mol), and Au_2I_2 (65.2 kJ/mol) under the level of DKH2-CCSD(T)/cc-pVTZ-DK/SO, indicating that the dsp^2═dsp^2 coordinate Au═Au bond is weakened with the increased covalent Au−X interactions down the periodic table for halogens. The details are summarized in Supporting Information Sections 3.2 and 3.3.

Covalent Nature of Au^I···Au^I Attraction in Au_3F_3 and Au_4F_4. The coordinate covalent nature of closed-shell Au^I···Au^I attraction can be further demonstrated in the trimerization and tetramerization of AuF, where each Au atom adopts dsp^2 hybridization. In Figure 5a, we notice the competition between annular isomers (**3a**/**4a**) stabilized by covalent Au−F bonds and windmill-shaped structures (**3w**/**4w**) stabilized by Au^I···Au^I attractions, which is quite similar to the competition between **1r** and **1t**. **1t**/**3w**/**4w** are mainly polymerized by closed-shell Au−Au bonds rather than the covalent Au−F bonds, while **1r**/**3a**/**4a** are stabilized by Au−F bonds. Therefore, the Au−Au distance in **3w**/**4w** is closer than that in **3a**/**4a**.

Under the level of DKH2-CCSD(T)/cc-pVTZ-DK/SO, the potential energies of **3w** and **4w** are 69.4 kJ/mol and 160.0 kJ/mol higher than those of **3a** and **4a**, respectively, indicating that Au_nF_n with a higher degree of polymerization is more favored to be stabilized by covalent Au−F bonds. The parameters of the optimized structures are listed in Table 3.

Table 3. Bond Distance [R (Å)] of Au−Au and Au−F Bonds, Bond Angle [A (°)] of F−Au−Au for 3w/4w or F−Au−F for 3a/4a, NPA Charge [q_{Au} (e)] of Au, HOMO−LUMO Gaps [E_{HL} (eV)], MBO, and WBI of Au−Au and Au−F Bonds under the Level of ZORA-TPSS-D3/dhf-QZVPP-2c

structure	r (Å)	A (°)	q_{Au} (e)	E_{HL} (eV)	MBO	WBI
	Au−Au/Au−F				Au−Au/Au−F	Au−Au/Au−F
3w	2.53/1.92	175.3	0.54	1.54	0.70/0.74	1.35/1.50
3a	2.75/2.12	159.5	0.60	2.00	0.21/0.45	0.79/0.95
4w	2.53/1.94	179.5	0.56	1.76	0.65/0.66	1.23/1.44
4a	2.88/2.06	178.9	0.58	2.55	0.19/0.47	0.68/1.01

Different from **1z**, the Au−Au bonds are single coordinate bonds in **3w**/**4w** rather than the coordinate double bond in **1z**. Compared with WBI/MBO results of Au_2F_2 (**1z**), the covalent interactions of Au−Au and Au−F bonds are weakened in **3w**/**4w**, reflected by the results in Table 3.

We confirm the structural transformation from windmill-shaped structures to annular structures through the corresponding transition states based on the relaxed energy scan under the level of TPSS-D3(BJ)/dhf-QZVPP in Supporting Information Figure S8, where the energy barriers for the isomerizations of **3w** → **3a** and **4w** → **4a** are 130.5 and 51.1 kJ/mol, respectively.

Detailed AdNDP analyses for **3w** and **4w** are listed in Figure 5b,c. Obviously, in Au_3F_3 (**3w**) and Au_4F_4 (**4w**), each Au atom

https://doi.org/10.1021/acs.inorgchem.1c03151
Inorg. Chem. 2022, 61, 1051−1058

Table 4. EDA (in kJ/mol) in $(AuX)_2$ (X = F, Cl, Br, I, and NH_2), Au_3F_3, and Au_4F_4 at the ZORA-TPSS-D3(BJ)/TZ2P Level in the ADF Package (V2014.01), Except the T-Shaped Au_2F_2 is Divided into One Au Atom and F_2Au Fragment, Others are based on the Definition of the Reaction of $(AuX)_n \rightarrow n$ AuX

structure		E_{pauli} [a]	E_{elst} [b]	E_{orb} [c]	E_{disp} [d]	E_{total} [e]	$E_{Coulomb}$ [f]
Au_2F_2	C_{2v}(**1t**)	512.2	−326.4	−424.1	−8.1	−246.4	
	C_{2h}(**1z**)	277.4	−184.1	−234.7	−6.8	−148.20	34.1
$Au_2(NH_2)_2$	C_{2h}(**Nz1**)	344.6	−282.0	−221.3	−8.4	−167.0	13.7
	C_{2h}(**Nz2**)	300.9	−239.3	−169.9	−8.5	−116.7	7.6
Au_3F_3	C_{3h}(**3w**)	607.5	−355.6	−654.3	−20.5	−422.8	34.9
Au_4F_4	C_{4h}(**4w**)	902.7	−591.2	−883.1	−39.7	−611.2	73.0
Au_2Cl_2	C_{2h}(**2z**) [g]	263.7	−186.5	−190.1	−9.5	−122.4	14.9
Au_2Br_2	C_{2h}(**3z**) [g]	261.0	−192.4	−178.2	−10.5	−120.1	9.4
Au_2I_2	C_{2h}(**4z**) [g]	266.8	−200.6	−167.8	−11.9	−113.5	3.8

[a] E_{Pauli} is the Pauli-repulsive orbital interaction between the same-spin electrons. [b] E_{elst} describes the electrostatic attraction. [c] E_{orb} is the orbital interaction, including the interaction between occupied orbitals on one fragment with unoccupied orbitals on the other fragment, including donor−acceptor interactions and polarization. [d] E_{disp} refers to van der Waal's dispersion. [e] E_{total} is defined as the summation of the electrostatic interactions (including E_{Pauli} and E_{elec}), covalent interactions (E_{orb}), and van der Waal's dispersion (E_{disp}). [f] $E_{Coulomb}$ is the electrostatic interaction calculated using Coulomb's equation (eqs 1 and 2). [g] Structures of Au_2Cl_2, Au_2Br_2, and Au_2I_2 are shown in Figure S2.

adopts inequivalent dsp^2 hybridization to form one F−Au σ bond, one F → Au coordinate bond, and two single coordinate Au−Au bonds to connect with two neighbored Au atoms. Similar to the Lewis structures of Au_3F_3 shown in Figure 5d, with dsp^2 hybridization, Au1 acts as not only the LPs-donor of the Au2 atom but also the LPs-acceptor of the Au3 atom. Similarly, Au2 is the LPs-donor of Au3 and the LPs-acceptor of Au1, while Au3 is the LPs-donor of Au1 and the LPs-donor of Au2 to form a windmill-shaped structure. It is exactly similar in windmill-shape Au_4F_4 shown in Figure 5d, where the LPs for each Au atom are donated and accepted in a head-to-tail manner (Au1 → Au2 ↑ ↓ Au4 ← Au3) to form a windmill-shape tetramer of AuF. The bonding analyses of **3a** and **4a** are summarized in Supporting Information Section 7.3.

The nature of closed-shell $Au^I \cdots Au^I$ attraction is the coordinate covalent interaction between Lewis acid and Lewis base (Figure 5d). The energy of polymerization is defined as the equation of $E_b = [E(Au_nF_n) - n^*E(AuF)]/n$, where n is the degree of polymerization. E_b is 101.5 kJ/mol for Au_3F_3 and 116.8 kJ/mol for Au_4F_4, suggesting that the stability is increased with an increasing degree of polymerization.

RDG analyses are plotted in Figure 5e, where the peak at −0.082 suggests that the strength of aurophilic interactions of Au_3F_3 (**3w**) is close to that of Au_4F_4 (**4w**). Compared with the RDG plots of Au_2F_2 (**1z**) shown in Figure 2h, the Au−Au (−0.082) and Au−F (−0.142/−0.138) interactions in **3w** and **4w** are weakened apparently caused by the single coordinate Au−Au bond, rather than the coordinate covalent double bond. The decreased Au−F interactions also suggest that the ligand−metal interaction is weakened with the increased degree of polymerization and gradually unconsolidated dsp^2 hybridization of Au, which is consistent with the MBO/WBI results shown in Table 3.

Finally, in order to confirm the coordinate covalent nature of aurophilicity, we accomplish the EDA for different aurophilic-favored polymers of $(AuX)_2$ (X = F, Cl, Br, I, and NH_2), Au_3F_3 (**3w**), and Au_4F_4 (**4w**) using the Amsterdam Density Functional (ADF 2014.01) program (Table 4). We define that each polymer is polymerized from the respective monomers, except for the Au_2F_2 (**1t**) isomer, which is polymerized from the fragments of F_2Au and Au. All the EDA results are shown in Table 4.

Based on the results in Table 4, all the values of E_{total} are negative, indicating the polymerizations from the closed-shell fragments are thermodynamically favored.

As for the Coulomb interactions ($E_{Coulomb}$), we applied Coulomb's equation (eqs 1 and 2) to calculate the electrostatic interaction between Au atoms, based on the atomic charge (q_A and q_B) and the distance of the atom (r_{AB}).

$$F_{AB} = k\frac{q_A q_B}{r_{AB}^2} \quad (1)$$

$$E_{coulomb}(AB) = F_{AB} r_{AB} \quad (2)$$

We have calculated the electrostatic interactions in the molecule based on eqs 1 and 2, which are the same tendency of the summary of the Pauli-repulsive orbital interactions (E_{pauli}) and electrostatic attractions (E_{elst}). All the details are listed in Supporting Information Table S6. Based on the results, both the Coulomb interactions between two Au atoms and total electrostatic interactions are positive, indicating that the Coulomb interactions are the repulsive components in the closed-shell interactions.

However, the attractions between the fragments are dominated by the covalent interactions (E_{orb}), which is strong enough to balance the electrostatic repulsions to form a stable Au−Au bond. Therefore, the nature of closed-shell $Au^I \cdots Au^I$ attraction is the covalent bond.

CONCLUSIONS

In summary, it is a new perspective to view the closed-shell $Au^I \cdots Au^I$ attractions as the coordinate covalent bond, based on the research of T-shaped Au_2F_2, zigzag M_2X_2, where M = Au, Ag, Cu, and X = F, Cl, Br, I, or NH_2 and windmill-shaped Au_3F_3/Au_4F_4, where the closed-shell attraction is actually the coordinate interactions between Lewis acid and Lewis base. Especially in the coordinate Au−Au bond in the zigzag Au_2F_2, each Au^I species is demonstrated as both Lewis acid and base.

As for the stability of the coordinate Au−Au bond, we demonstrate that the ligand with stronger electronegativity is favorable for the activation of the 5d electrons of the Au atom. The closed-shell attraction is enhanced with consolidated dsp or dsp^2 hybridization of the Au atom, which can be tuned by the relationship between the ligand and Au. This viewpoint is

https://doi.org/10.1021/acs.inorgchem.1c03151
Inorg. Chem. 2022, 61, 1051−1058

extended to successfully explain the closed-shell attraction of windmill-shaped Au_3F_3 and Au_4F_4.

Our work provides a rather simple but clear-cut example, where mysterious $Au^I\cdots Au^I$ attractions can be possibly explained by the covalent bond theory. Studies that focus on a more detailed explanation of more complex clusters containing $Au^I\cdots Au^I$ attractions are currently under progress.

■ ASSOCIATED CONTENT

Supporting Information

The Supporting Information is available free of charge at https://pubs.acs.org/doi/10.1021/acs.inorgchem.1c03151.

Theoretical methods based on the benchmark study, global search, relaxed energy scan, ELF and LOL contour plots, RDG analyses, QTAIM analyses, components of the Au−Au bonds in the dimers, and the Cartesian coordinates (in Å) of all structures (PDF)

■ AUTHOR INFORMATION

Corresponding Authors

Kun Wang − *Department of Chemistry, Anhui University, Hefei, Anhui 230601, PR China;* orcid.org/0000-0003-2175-1105; Email: wangkun@ahu.edu.cn

Longjiu Cheng − *Department of Chemistry, Anhui University, Hefei, Anhui 230601, PR China; Laboratory of Structure and Functional Regulation of Hybrid Materials (Anhui University), Ministry of Education, Hefei 230601, PR China;* orcid.org/0000-0001-7086-6190; Email: clj@ustc.edu

Authors

Xinlei Yu − *Department of Chemistry, Anhui University, Hefei, Anhui 230601, PR China*

Dan Li − *Department of Chemistry, Anhui University, Hefei, Anhui 230601, PR China*

Tao Xia − *Department of Chemistry, Anhui University, Hefei, Anhui 230601, PR China*

Chang Xu − *Department of Chemistry, Anhui University, Hefei, Anhui 230601, PR China*

Zhenyu Wu − *Department of Chemistry, Anhui University, Hefei, Anhui 230601, PR China*

Complete contact information is available at: https://pubs.acs.org/10.1021/acs.inorgchem.1c03151

Author Contributions

X.Y., K.W., and L.C. designed research; X.Y., D.L., and L.C. analyzed data; X.Y., D.L., K.W., T.X., C.X., Z.W., and L.C. performed research; X.Y., K.W., and L.C. wrote the manuscript.

Funding

This research was made possible as a result of generous grants from the National Natural Science Foundation of China (21873001, 21701001), the Foundation of Distinguished Young Scientists of Anhui Province, and the Natural Science Research Project of Anhui Province (KJ2020ZD04).

Notes

The authors declare no competing financial interest.

■ ACKNOWLEDGMENTS

The calculations are carried out at the High-Performance Computing Center of Anhui University.

■ REFERENCES

(1) Koirala, P.; Willis, M.; Kiran, B.; Kandalam, A. K.; Jena, P. Superhalogen properties of fluorinated coinage metal clusters. *J. Phys. Chem. C* **2010**, *114*, 16018−16024.

(2) Tian, Z. M.; Cheng, L. J. Perspectives on the energy landscape of Au−Cl binary systems from the structural phase diagram of Au_xCl_y ($x + y = 20$). *Phys. Chem. Chem. Phys.* **2015**, *17*, 13421−13428.

(3) Xu, C. Q.; Xiong, X. G.; Li, W. L.; Li, J. Periodicity and Covalency of $[MX_2]^-$ (M = Cu, Ag, Au, Rg; X = H, Cl, CN) Complexes. *Eur. J. Inorg. Chem.* **2016**, *2016*, 1395−1404.

(4) Ma, Y.; Bian, S.; Shi, Y. Y.; Fan, X. T.; Kong, X. L. Size Effect on Aurophilic Interaction in Gold-Chloride Cluster Anions of $Au_nCl_{n+1}^-$ ($2 \le n \le 7$). *ACS Omega* **2019**, *4*, 650−654.

(5) Tian, Z. M.; Song, C. F.; Wang, C.; Liu, Z. D.; Liao, R. B. Theoretical characterization of $(CuF)_n$ (n = 1−12) clusters. *Comput. Theor. Chem.* **2019**, *1157*, 28−33.

(6) Pang, X. X.; Guo, M. G.; Wang, Z. F.; Wang, F. Low-lying states of MX_2 (M = Ag, Au; X = Cl, Br and I) with coupled-cluster approaches: effect of the basis set, high level correlation and spin−orbit coupling. *Phys. Chem. Chem. Phys.* **2020**, *22*, 26178−26188.

(7) Li, X. Y.; Cai, J. X. Electron density properties and metallophilic interactions of gold halides AuX_2 and Au_2X (X = F−I): Ab Initio calculations. *Int. J. Quantum Chem.* **2016**, *116*, 1350−1357.

(8) Liu, Y.; Tian, Z. M.; Cheng, L. J. Size evolution and ligand effects on the structures and stability of $(AuL)_n$ (L = Cl, SH, SCH_3, PH_2, $P(CH_3)_2$, n = 1−13) clusters. *RSC Adv.* **2016**, *6*, 4705−4712.

(9) Li, X. Y. Electron density properties and metallophilic interactions of coinage metal halides M_2X_2 (M = Cu, Ag and Au, X = F−I): Ab initio calculation. *Mater. Res. Express* **2016**, *3*, No. 115702.

(10) Li, X. Y.; Cai, J. X. On the covalence in coinage-metal halides M_3X_3 (M = Cu, Ag and Au, X = F−I). *Mol. Phys.* **2017**, *115*, 1544−1554.

(11) Yu, S.; Kumar, P.; Ward, J. S.; Frontera, A.; Rissanen, K. A "nucleophilic" iodine in a halogen-bonded iodonium complex manifests an unprecedented $I^+\cdots Ag^+$ interaction. *Chem* **2021**, *7*, 948−958.

(12) Rabilloud, F. Structure and Bonding in Coinage Metal Halide Clusters M_nX_n, M = Cu, Ag, Au; X = Br, I; n = 1−6. *J. Phys. Chem. A* **2012**, *116*, 3474−3480.

(13) Schwerdtfeger, P.; McFeaters, J. S.; Liddell, M. J.; Hrušák, J.; Schwarz, H. Spectroscopic properties for the ground states of AuF, AuF^+, AuF_2, and Au_2F_2: A pseudopotential scalar relativistic Møller−Plesset and coupled-cluster study. *J. Chem. Phys.* **1995**, *103*, 245−252.

(14) Rabilloud, F. Structure and stability of coinage metal fluoride and chloride clusters (M_nF_n and M_nCl_n, M = Cu, Ag, or Au; n = 1−6). *J. Comput. Chem.* **2012**, *33*, 2083−2091.

(15) Pyykkö, P.; Li, J.; Runeberg, N. Predicted ligand dependence of the Au (I)...Au (I) attraction in $(XAuPH_3)_2$. *Chem. Phys. Lett.* **1994**, *218*, 133−138.

(16) Andris, E.; Andrikopoulos, P. C.; Schulz, J.; Turek, J.; Růžička, A.; Roithová, J.; Rulíšek, L. Aurophilic Interactions in [(L) AuCl]... [(L′) AuCl] Dimers: Calibration by Experiment and Theory. *J. Am. Chem. Soc.* **2018**, *140*, 2316−2325.

(17) Housecroft, C. E. Gold. *Coord. Chem. Rev.* **1992**, *115*, 117−140.

(18) Mirzadeh, N.; Privér, S. H.; Blake, A. J.; Schmidbaur, H.; Bhargava, S. K. Innovative Molecular Design Strategies in Materials Science Following the Aurophilicity Concept. *Chem. Rev.* **2020**, *120*, 7551−7591.

(19) Moreno-Alcántar, G.; Turcio-García, L.; Guevara-Vela, J. M.; Romero-Montalvo, E.; Rocha-Rinza, T.; Pendás, Á. M.; Flores-Álamo, M.; Torrens, H. Directing the Crystal Packing in Triphenylphosphine Gold (I) Thiolates by Ligand Fluorination. *Inorg. Chem.* **2020**, *59*, 8667−8677.

(20) Straube, A.; Coburger, P.; Dütsch, L.; Hey-Hawkins, E. Triple the fun: tris (ferrocenyl) arene-based gold (I) complexes for redox-switchable catalysis. *Chem. Sci.* **2020**, *11*, 10657−10668.

(21) Zeman, C. J., IV; Shen, Y. H.; Heller, J. K.; Abboud, K. A.; Schanze, K. S.; Veige, A. S. Excited-State Turn-On of Aurophilicity

and Tunability of Relativistic Effects in a Series of Digold Triazolates Synthesized via iClick. *J. Am. Chem. Soc.* **2020**, *142*, 8331−8341.
(22) Scherbaum, F.; Grohmann, A.; Huber, B.; Krüger, C.; Schmidbaur, H. "Aurophilicity" as a consequence of relativistic effects: the hexakis (triphenylphosphaneaurio) methane dication $[(Ph_3PAu)_6C]_2^{\oplus}$. *Angew. Chem., Int. Ed. Engl.* **1988**, *27*, 1544−1546.
(23) Pyykkö, P.; Zaleski-Ejgierd, P. Basis-set limit of the aurophilic attraction using the MP2 method: The examples of $[ClAuPH_3]_2$ dimer and $[P(AuPH_3)_4]^+$ ion. *J. Chem. Phys.* **2008**, *128*, 124309.
(24) Pyykkö, P. Strong closed-shell interactions in inorganic chemistry. *Chem. Rev.* **1997**, *97*, 597−636.
(25) Pyykkö, P. Theoretical chemistry of gold. *Angew. Chem., Int. Ed.* **2004**, *43*, 4412−4456.
(26) Pyykkö, P. Theoretical chemistry of gold. II. *Inorg. Chim. Acta* **2005**, *358*, 4113−4130.
(27) Pyykkö, P. Theoretical chemistry of gold. III. *Chem. Soc. Rev.* **2008**, *37*, 1967−1997.
(28) Gagliardi, L.; Pyykkö, P. Theoretical Search for Very Short Metal−Actinide Bonds: NUIr and Isoelectronic Systems. *Angew. Chem., Int. Ed.* **2004**, *116*, 1599−1602.
(29) Schmidbaur, H.; Schier, A. Mercurophilic Interactions. *Organometallics* **2015**, *34*, 2048−2066.
(30) Vellé, A.; Rodríguez-Santiago, L.; Sodupe, M.; Sanz Miguel, P. J. Enhanced Metallophilicity in Metal−Carbene Systems: Stronger Character of Aurophilic Interactions in Solution. *Chem. − Eur. J.* **2020**, *26*, 997−1002.
(31) Zheng, Q.; Borsley, S.; Nichol, G. S.; Duarte, F.; Cockroft, S. L. The energetic significance of metallophilic interactions. *Angew. Chem., Int. Ed.* **2019**, *58*, 12617−12623.
(32) Sculfort, S.; Braunstein, P. Intramolecular d^{10}−d^{10} interactions in heterometallic clusters of the transition metals. *Chem. Soc. Rev.* **2011**, *40*, 2741−2760.
(33) Echeverría, J. In (iii)··· In (iii) short contacts: an unnoticed metallophilic interaction? *Chem. Commun.* **2018**, *54*, 6312−6315.
(34) Schmidbaur, H.; Schier, A. Argentophilic interactions. *Angew. Chem., Int. Ed.* **2015**, *54*, 746−784.
(35) Ni, W. X.; Qiu, Y. M.; Li, M.; Zheng, J.; Sun, R. W. Y.; Zhan, S. Z.; Ng, S. W.; Li, D. Metallophilicity-driven dynamic aggregation of a phosphorescent gold (I)−silver (I) cluster prepared by solution-based and mechanochemical approaches. *J. Am. Chem. Soc.* **2014**, *136*, 9532−9535.
(36) Donamaría, R.; Lippolis, V.; López-de-Luzuriaga, J. M.; Monge, M.; Nieddu, M.; Olmos, M. E. Structural and Luminescence Properties of Heteronuclear Gold (I)/Thallium (I) Complexes Featuring Metallophilic Interactions Tuned by Quinoline Pendant Arm Derivatives of Mixed Donor Macrocycles. *Inorg. Chem.* **2020**, *59*, 6398−6409.
(37) Jiang, Y.; Alvarez, S.; Hoffmann, R. Binuclear and polymeric gold (I) complexes. *Inorg. Chem.* **1985**, *24*, 749−757.
(38) Mehrotra, P. K.; Hoffmann, R. Copper (I)-copper (I) interactions. Bonding relationships in d^{10}−d^{10} systems. *Inorg. Chem.* **1978**, *9*, 2187−2189.
(39) Pyykkö, P.; Zhao, Y. F. Ab initio calculations on the $(ClAuPH_3)_2$ dimer with relativistic pseudopotential: Is the "aurophilic attraction" a correlation effect? *Angew. Chem., Int. Ed. Engl.* **1991**, *30*, 604−605.
(40) Magnko, L.; Schweizer, M.; Rauhut, G.; Schütz, M.; Stoll, H.; Werner, H. J. A comparison of metallophilic attraction in $(X−M−PH_3)_2$ (M = Cu, Ag, Au; X = H, Cl). *Phys. Chem. Chem. Phys.* **2002**, *4*, 1006−1013.
(41) Otero-de-la-Roza, A.; Mallory, J. D.; Johnson, E. R. Metal-lophilic interactions from dispersion-corrected density-functional theory. *J. Chem. Phys.* **2014**, *140*, No. 18A504.
(42) O'Grady, E.; Kaltsoyannis, N. Does metallophilicity increase or decrease down group 11? Computational investigations of $[Cl−M−PH_3]_2$ (M = Cu, Ag, Au, [111]). *Phys. Chem. Chem. Phys.* **2004**, *6*, 680−687.
(43) Brands, M. B.; Nitsch, J.; Guerra, C. F. Relevance of orbital interactions and Pauli repulsion in the metal−metal bond of coinage metals. *Inorg. Chem.* **2018**, *57*, 2603−2608.
(44) Wan, Q. Y.; Yang, J.; To, W. P.; Che, C. M. Strong metal−metal Pauli repulsion leads to repulsive metallophilicity in closed-shell d^8 and d^{10} organometallic complexes. *Proc. Natl. Acad. Sci. U. S. A.* **2021**, *118*, No. e2019265118.
(45) Apra, E.; Bylaska, E. J.; De Jong, W. A.; Govind, N.; Kowalski, K.; Straatsma, T. P.; Valiev, M.; van Dam, H. J.; Alexeev, Y.; Anchell, J. NWChem: Past, present, and future. *J. Chem. Phys.* **2020**, *152*, 184102.
(46) Tao, J. M.; Perdew, J. P.; Staroverov, V. N.; Scuseria, G. E. Climbing the density functional ladder: Nonempirical meta−generalized gradient approximation designed for molecules and solids. *Phys. Rev. Lett.* **2003**, *91*, No. 146401.
(47) Weigend, F.; Ahlrichs, R. Balanced basis sets of split valence, triple zeta valence and quadruple zeta valence quality for H to Rn: Design and assessment of accuracy. *Phys. Chem. Chem. Phys.* **2005**, *7*, 3297−3305.
(48) Weigend, F.; Baldes, A. Segmented contracted basis sets for one-and two-component Dirac−Fock effective core potentials. *J. Chem. Phys.* **2010**, *133*, 174102.
(49) Figgen, D.; Rauhut, G.; Dolg, M.; Stoll, H. Energy-consistent pseudopotentials for group 11 and 12 atoms: adjustment to multi-configuration Dirac−Hartree−Fock data. *Chem. Phys.* **2005**, *311*, 227−244.
(50) Lenthe, E. V.; Baerends, E. J.; Snijders, J. G. Relativistic regular two-component Hamiltonians. *J. Chem. Phys.* **1993**, *99*, 4597−4610.
(51) Werner, H. J.; Knowles, P. J.; Knizia, G.; Manby, F. R.; Schütz, M. Molpro: a general-purpose quantum chemistry program package. *WIREs Comput. Mol. Sci.* **2012**, *2*, 242−253.
(52) Werner, H. J.; Knowles, P. J.; Manby, F. R.; Black, J. A.; Doll, K.; Heßelmann, A.; Kats, D.; Köhn, A.; Korona, T.; Kreplin, D. A. The Molpro quantum chemistry package. *J. Chem. Phys.* **2020**, *152*, 144107.
(53) Silvi, B.; Savin, A. Classification of chemical bonds based on topological analysis of electron localization functions. *Nature* **1994**, *371*, 683−686.
(54) Johnson, E. R.; Keinan, S.; Mori-Sánchez, P.; Contreras-García, J.; Cohen, A. J.; Yang, W. Revealing noncovalent interactions. *J. Am. Chem. Soc.* **2010**, *132*, 6498−6506.
(55) Mayer, I. Charge, bond order and valence in the Ab initio SCF theory. *Chem. Phys. Lett.* **1983**, *97*, 270−274.
(56) Mayer, I. Bond order and valence: Relations to Mulliken's population analysis. *Int. J. Quantum Chem.* **1984**, *26*, 151−154.
(57) Wiberg, K. B. Application of the pople-santry-segal CNDO method to the cyclopropylcarbinyl and cyclobutyl cation and to bicyclobutane. *Tetrahedron* **1968**, *24*, 1083−1096.
(58) Frisch, M.; Trucks, G.; Schlegel, H.; Scuseria, G.; Robb, M.; Cheeseman, J.; Scalmani, G.; Barone, V.; Petersson, G.; Nakatsuji, H. *Gaussian 16 Revision C. 01*; Gaussian Inc.: Wallingford, CT, 2016.
(59) Lu, T.; Chen, F. W. Multiwfn: a multifunctional wavefunction analyzer. *J. Comput. Chem.* **2012**, *33*, 580−592.
(60) Humphrey, W.; Dalke, A.; Schulten, K. VMD: visual molecular dynamics. *J. Mol. Graphics* **1996**, *14*, 33−38.
(61) Zubarev, D. Y.; Boldyrev, A. I. Developing paradigms of chemical bonding: adaptive natural density partitioning. *Phys. Chem. Chem. Phys.* **2008**, *10*, 5207−5217.
(62) Amsterdam Density Functional (ADF) 2014.01 Version, Theoretical Chemistry, Vrije Universiteit: Amsterdam. The Netherlands, http://www.scm.com.
(63) Pyykkö, P.; Mendizabal, F. Theory of the d^{10}−d^{10} Closed-Shell Attraction: 2. Long-Distance Behaviour and Nonadditive Effects in Dimers and Trimers of Type $[(X-Au-L_n)]$ (n = 2, 3; X = Cl, I, H; L = PH_3, PMe_3, −N≡CH). *Chem. − Eur. J.* **1997**, *3*, 1458−1465.
(64) Li, W. L.; Liu, H. T.; Jian, T.; Lopez, G. V.; Piazza, Z. A.; Huang, D. L.; Chen, T. T.; Su, J.; Yang, P.; Chen, X.; Wang, L. S.; Li, J. Bond-bending isomerism of $Au_2I_3^-$: competition between covalent bonding and aurophilicity. *Chem. Sci.* **2016**, *7*, 475−481.

https://doi.org/10.1021/acs.inorgchem.1c03151
Inorg. Chem. 2022, 61, 1051−1058